

Measurement of the W Mass using $W \rightarrow e\nu$ decays at D \emptyset

The D \emptyset Collaboration¹
(July 1996)

Preliminary measurements of the W boson mass from $W \rightarrow e\nu$ decays produced in $p\bar{p}$ collisions at $\sqrt{s} = 1.8$ TeV using the D \emptyset detector are presented. The analysis uses events with electrons in the central region ($|\eta| < 1.2$). The technique for determining the mass and its systematic errors is discussed.

S. Abachi,¹⁴ B. Abbott,²⁸ M. Abolins,²⁵ B.S. Acharya,⁴³ I. Adam,¹² D.L. Adams,³⁷ M. Adams,¹⁷
S. Ahn,¹⁴ H. Aihara,²² J. Alitti,⁴⁰ G. Alvarez,¹⁸ G.A. Alves,¹⁰ E. Amidi,²⁹ N. Amos,²⁴
E.W. Anderson,¹⁹ S.H. Aronson,⁴ R. Astur,⁴² R.E. Avery,³¹ M.M. Baarmand,⁴² A. Baden,²³
V. Balamurali,³² J. Balderston,¹⁶ B. Baldin,¹⁴ S. Banerjee,⁴³ J. Bantly,⁵ J.F. Bartlett,¹⁴
K. Bazizi,³⁹ J. Bendich,²² S.B. Beri,³⁴ I. Bertram,³⁷ V.A. Bezzubov,³⁵ P.C. Bhat,¹⁴
V. Bhatnagar,³⁴ M. Bhattacharjee,¹³ A. Bischoff,⁹ N. Biswas,³² G. Blazey,¹⁴ S. Blessing,¹⁵
P. Bloom,⁷ A. Bohnlein,¹⁴ N.I. Bojko,³⁵ F. Borcherding,¹⁴ J. Borders,³⁹ C. Boswell,⁹
A. Brandt,¹⁴ R. Brock,²⁵ A. Bross,¹⁴ D. Buchholz,³¹ V.S. Burtovoi,³⁵ J.M. Butler,³
W. Carvalho,¹⁰ D. Casey,³⁹ H. Castilla-Valdez,¹¹ D. Chakraborty,⁴² S.-M. Chang,²⁹
S.V. Chekulaev,³⁵ L.-P. Chen,²² W. Chen,⁴² S. Choi,⁴¹ S. Chopra,²⁴ B.C. Choudhary,⁹
J.H. Christenson,¹⁴ M. Chung,¹⁷ D. Claes,⁴² A.R. Clark,²² W.G. Cobau,²³ J. Cochran,⁹
W.E. Cooper,¹⁴ C. Cretzinger,³⁹ D. Cullen-Vidal,⁵ M.A.C. Cummings,¹⁶ D. Cutts,⁵ O.I. Dahl,²²
K. De,⁴⁴ M. Demarteau,¹⁴ N. Denisenko,¹⁴ D. Denisov,¹⁴ S.P. Denisov,³⁵ H.T. Diehl,¹⁴
M. Diesburg,¹⁴ G. Di Loreto,²⁵ R. Dixon,¹⁴ P. Draper,⁴⁴ J. Drinkard,⁸ Y. Ducros,⁴⁰
S.R. Dugad,⁴³ D. Edmunds,²⁵ J. Ellison,⁹ V.D. Elvira,⁴² R. Engelmann,⁴² S. Eno,²³ G. Eppley,³⁷
P. Ermolov,²⁶ O.V. Eroshin,³⁵ V.N. Evdokimov,³⁵ S. Fahey,²⁵ T. Fahland,⁵ M. Fatyga,⁴
M.K. Fatyga,³⁹ J. Featherly,⁴ S. Feher,¹⁴ D. Fein,² T. Ferbel,³⁹ G. Finocchiaro,⁴² H.E. Fisk,¹⁴
Y. Fisyak,⁷ E. Flattum,²⁵ G.E. Forden,² M. Fortner,³⁰ K.C. Frame,²⁵ P. Franzini,¹² S. Fuess,¹⁴
E. Gallas,⁴⁴ A.N. Galyaev,³⁵ T.L. Geld,²⁵ R.J. Genik II,²⁵ K. Genser,¹⁴ C.E. Gerber,¹⁴
B. Gibbard,⁴ V. Glebov,³⁹ S. Glenn,⁷ J.F. Glicenstein,⁴⁰ B. Gobbi,³¹ M. Goforth,¹⁵
A. Goldschmidt,²² B. Gómez,¹ G. Gomez,²³ P.I. Goncharov,³⁵ J.L. González Solís,¹¹ H. Gordon,⁴
L.T. Goss,⁴⁵ N. Graf,⁴ P.D. Grannis,⁴² D.R. Green,¹⁴ J. Green,³⁰ H. Greenlee,¹⁴ G. Griffin,⁸
N. Grossman,¹⁴ P. Grudberg,²² S. Grünendahl,³⁹ W.X. Gu,^{14,*} G. Guglielmo,³³ J.A. Guida,²
J.M. Guida,⁵ W. Guryn,⁴ S.N. Gurzhiev,³⁵ P. Gutierrez,³³ Y.E. Gutnikov,³⁵ N.J. Hadley,²³
H. Haggerty,¹⁴ S. Hagopian,¹⁵ V. Hagopian,¹⁵ K.S. Hahn,³⁹ R.E. Hall,⁸ S. Hansen,¹⁴
R. Hatcher,²⁵ J.M. Hauptman,¹⁹ D. Hedin,³⁰ A.P. Heinson,⁹ U. Heintz,¹⁴
R. Hernández-Montoya,¹¹ T. Heuring,¹⁵ R. Hirosky,¹⁵ J.D. Hobbs,¹⁴ B. Hoeneisen,^{1,†}
J.S. Hoftun,⁵ F. Hsieh,²⁴ Tao Hu,^{14,*} Ting Hu,⁴² Tong Hu,¹⁸ T. Huehn,⁹ S. Igarashi,¹⁴ A.S. Ito,¹⁴
E. James,² J. Jaques,³² S.A. Jerger,²⁵ J.Z.-Y. Jiang,⁴² T. Joffe-Minor,³¹ H. Johari,²⁹ K. Johns,²
M. Johnson,¹⁴ H. Johnstad,²⁹ A. Jonckheere,¹⁴ M. Jones,¹⁶ H. Jöstlein,¹⁴ S.Y. Jun,³¹
C.K. Jung,⁴² S. Kahn,⁴ G. Kalbfleisch,³³ J.S. Kang,²⁰ R. Kehoe,³² M.L. Kelly,³² L. Kerth,²²
C.L. Kim,²⁰ S.K. Kim,⁴¹ A. Klatchko,¹⁵ B. Klima,¹⁴ B.I. Klochkov,³⁵ C. Klopfenstein,⁷
V.I. Klyukhin,³⁵ V.I. Kochetkov,³⁵ J.M. Kohli,³⁴ D. Koltick,³⁶ A.V. Kostritskiy,³⁵ J. Kotcher,⁴

¹Submitted to the 28th International Conference on High Energy Physics, Warsaw, Poland, 25-31 July 1996.

J. Kourlas,²⁸ A.V. Kozelov,³⁵ E.A. Kozlovski,³⁵ M.R. Krishnaswamy,⁴³ S. Krzywdzinski,¹⁴
 S. Kunori,²³ S. Lami,⁴² G. Landsberg,¹⁴ J-F. Lebrat,⁴⁰ A. Leflat,²⁶ H. Li,⁴² J. Li,⁴⁴ Y.K. Li,³¹
 Q.Z. Li-Demarteau,¹⁴ J.G.R. Lima,³⁸ D. Lincoln,²⁴ S.L. Linn,¹⁵ J. Linnemann,²⁵ R. Lipton,¹⁴
 Y.C. Liu,³¹ F. Lobkowicz,³⁹ S.C. Loken,²² S. Lökös,⁴² L. Lueking,¹⁴ A.L. Lyon,²³
 A.K.A. Maciel,¹⁰ R.J. Madaras,²² R. Madden,¹⁵ L. Magaña-Mendoza,¹¹ S. Mani,⁷ H.S. Mao,^{14,*}
 R. Markeloff,³⁰ L. Markosky,² T. Marshall,¹⁸ M.I. Martin,¹⁴ B. May,³¹ A.A. Mayorov,³⁵
 R. McCarthy,⁴² T. McKibben,¹⁷ J. McKinley,²⁵ T. McMahon,³³ H.L. Melanson,¹⁴
 J.R.T. de Mello Neto,³⁸ K.W. Merritt,¹⁴ H. Miettinen,³⁷ A. Mincer,²⁸ J.M. de Miranda,¹⁰
 C.S. Mishra,¹⁴ N. Mokhov,¹⁴ N.K. Mondal,⁴³ H.E. Montgomery,¹⁴ P. Mooney,¹ H. da Motta,¹⁰
 M. Mudan,²⁸ C. Murphy,¹⁷ F. Nang,⁵ M. Narain,¹⁴ V.S. Narasimham,⁴³ A. Narayanan,²
 H.A. Neal,²⁴ J.P. Negret,¹ E. Neis,²⁴ P. Nemethy,²⁸ D. Nešić,⁵ M. Nicola,¹⁰ D. Norman,⁴⁵
 L. Oesch,²⁴ V. Oguri,³⁸ E. Oltman,²² N. Oshima,¹⁴ D. Owen,²⁵ P. Padley,³⁷ M. Pang,¹⁹
 A. Para,¹⁴ C.H. Park,¹⁴ Y.M. Park,²¹ R. Partridge,⁵ N. Parua,⁴³ M. Paterno,³⁹ J. Perkins,⁴⁴
 A. Peryshkin,¹⁴ M. Peters,¹⁶ H. Piekarz,¹⁵ Y. Pischalnikov,³⁶ V.M. Podstavkov,³⁵ B.G. Pope,²⁵
 H.B. Prosper,¹⁵ S. Protopopescu,⁴ D. Pušeljić,²² J. Qian,²⁴ P.Z. Quintas,¹⁴ R. Raja,¹⁴
 S. Rajagopalan,⁴² O. Ramirez,¹⁷ M.V.S. Rao,⁴³ P.A. Rapidis,¹⁴ L. Rasmussen,⁴² S. Reucroft,²⁹
 M. Rijssenbeek,⁴² T. Rockwell,²⁵ N.A. Roe,²² P. Rubinov,³¹ R. Ruchti,³² J. Rutherford,²
 A. Sánchez-Hernández,¹¹ A. Santoro,¹⁰ L. Sawyer,⁴⁴ R.D. Schamberger,⁴² H. Schellman,³¹
 J. Sculli,²⁸ E. Shabalina,²⁶ C. Shaffer,¹⁵ H.C. Shankar,⁴³ R.K. Shivpuri,¹³ M. Shupe,²
 J.B. Singh,³⁴ V. Sirotenko,³⁰ W. Smart,¹⁴ A. Smith,² R.P. Smith,¹⁴ R. Smihur,³¹ G.R. Snow,²⁷
 J. Snow,³³ S. Snyder,⁴ J. Solomon,¹⁷ P.M. Sood,³⁴ M. Sosebee,⁴⁴ M. Souza,¹⁰ A.L. Spadafora,²²
 R.W. Stephens,⁴⁴ M.L. Stevenson,²² D. Stewart,²⁴ D.A. Stoianova,³⁵ D. Stoker,⁸ K. Streets,²⁸
 M. Strovink,²² A. Sznaider,¹⁰ P. Tamburello,²³ J. Tarazi,⁸ M. Tartaglia,¹⁴ T.L. Taylor,³¹
 J. Thompson,²³ T.G. Trippe,²² P.M. Tuts,¹² N. Varelas,²⁵ E.W. Varnes,²² P.R.G. Virador,²²
 D. Vititoe,² A.A. Volkov,³⁵ A.P. Vorobiev,³⁵ H.D. Wahl,¹⁵ G. Wang,¹⁵ J. Warchol,³² G. Watts,⁵
 M. Wayne,³² H. Weerts,²⁵ A. White,⁴⁴ J.T. White,⁴⁵ J.A. Wightman,¹⁹ J. Wilcox,²⁹ S. Willis,³⁰
 S.J. Wimpenny,⁹ J.V.D. Wirjawan,⁴⁵ J. Womersley,¹⁴ E. Won,³⁹ D.R. Wood,²⁹ H. Xu,⁵
 R. Yamada,¹⁴ P. Yamin,⁴ C. Yanagisawa,⁴² J. Yang,²⁸ T. Yasuda,²⁹ P. Yepes,³⁷ C. Yoshikawa,¹⁶
 S. Youssef,¹⁵ J. Yu,¹⁴ Y. Yu,⁴¹ Q. Zhu,²⁸ Z.H. Zhu,³⁹ D. Ziemska,¹⁸ A. Ziemska,¹⁸
 E.G. Zverev,²⁶ and A. Zylberstein⁴⁰

¹Universidad de los Andes, Bogotá, Colombia

²University of Arizona, Tucson, Arizona 85721

³Boston University, Boston, Massachusetts 02215

⁴Brookhaven National Laboratory, Upton, New York 11973

⁵Brown University, Providence, Rhode Island 02912

⁶Universidad de Buenos Aires, Buenos Aires, Argentina

⁷University of California, Davis, California 95616

⁸University of California, Irvine, California 92717

⁹University of California, Riverside, California 92521

¹⁰LAFEX, Centro Brasileiro de Pesquisas Físicas, Rio de Janeiro, Brazil

¹¹CINVESTAV, Mexico City, Mexico

¹²Columbia University, New York, New York 10027

¹³Delhi University, Delhi, India 110007

¹⁴Fermi National Accelerator Laboratory, Batavia, Illinois 60510

¹⁵Florida State University, Tallahassee, Florida 32306

¹⁶University of Hawaii, Honolulu, Hawaii 96822

¹⁷University of Illinois at Chicago, Chicago, Illinois 60607

¹⁸Indiana University, Bloomington, Indiana 47405

¹⁹Iowa State University, Ames, Iowa 50011

²⁰Korea University, Seoul, Korea

²¹Kyungsung University, Pusan, Korea
²²Lawrence Berkeley National Laboratory and University of California, Berkeley, California 94720
²³University of Maryland, College Park, Maryland 20742
²⁴University of Michigan, Ann Arbor, Michigan 48109
²⁵Michigan State University, East Lansing, Michigan 48824
²⁶Moscow State University, Moscow, Russia
²⁷University of Nebraska, Lincoln, Nebraska 68588
²⁸New York University, New York, New York 10003
²⁹Northeastern University, Boston, Massachusetts 02115
³⁰Northern Illinois University, DeKalb, Illinois 60115
³¹Northwestern University, Evanston, Illinois 60208
³²University of Notre Dame, Notre Dame, Indiana 46556
³³University of Oklahoma, Norman, Oklahoma 73019
³⁴University of Panjab, Chandigarh 16-00-14, India
³⁵Institute for High Energy Physics, 142-284 Protvino, Russia
³⁶Purdue University, West Lafayette, Indiana 47907
³⁷Rice University, Houston, Texas 77251
³⁸Universidade Estadual do Rio de Janeiro, Brazil
³⁹University of Rochester, Rochester, New York 14627
⁴⁰CEA, DAPNIA/Service de Physique des Particules, CE-SACLAY, France
⁴¹Seoul National University, Seoul, Korea
⁴²State University of New York, Stony Brook, New York 11794
⁴³Tata Institute of Fundamental Research, Colaba, Bombay 400005, India
⁴⁴University of Texas, Arlington, Texas 76019
⁴⁵Texas A&M University, College Station, Texas 77843

I. INTRODUCTION

The parameters of the electroweak sector of the Standard Model (1) can be taken to be the fine structure constant, the Fermi constant, and the mass of the Z boson, M_Z , all measured to a precision better than 0.01%. Higher order calculations then relate the mass of the W boson, M_W , and the weak mixing angle, ϑ_W , through these three parameters, the heavy fermion masses, and the Higgs boson mass. Within the Standard Model, a direct measurement of M_W thus constrains the allowed region for the top quark and Higgs masses. Alternatively, a precise measurement of the W mass in combination with measurements of $\sin^2 \vartheta_W$ provides a test of the Standard Model. The mass of the W boson has been measured recently in a number of experiments (2). We present here preliminary measurements based on data collected with the DØ detector during the 1992–1995 run at the Fermilab Tevatron collider. The run was subdivided into two periods, Run 1a from 1992–1993 and Run 1b from 1993–1995. Table 1 describes the relevant features of the two datasets.

Two components of the detector (3) are most relevant to this analysis. The central tracking system is used to reconstruct charged particle tracks and to reconstruct the vertices in the event. The calorimetry consists of one central and two end uranium liquid-argon calorimeters which measure the energy flow in the event over a pseudorapidity range $|\eta| \leq 4.2$ (4).

Since the longitudinal component of the neutrino momentum is not measured, the W invariant mass cannot be reconstructed. This implies that the mass of the W boson must be extracted from some other kinematic distribution, such as the electron energy

	Run 1a	Run 1b
Integrated luminosity	12.8 pb^{-1}	76 pb^{-1}
Maximum luminosity	$\approx 8 \times 10^{30} \text{ cm}^{-2} \text{ s}^{-1}$	$\approx 20 \times 10^{30} \text{ cm}^{-2} \text{ s}^{-1}$
Central $W \rightarrow e\nu$ candidates	7684	32856
Central-central $Z \rightarrow ee$ candidates	366	1562
Central-forward $Z \rightarrow ee$ candidates	281	1548

TABLE 1. Features of Run 1a and Run 1b $W \rightarrow e\nu$ and $Z \rightarrow ee$ data samples.

or transverse energy, the neutrino transverse momentum, or the transverse mass, defined as $M_T^2 = 2 |\vec{E}_T^e| |\vec{E}_T^\nu| (1 - \cos \varphi_{e\nu})$, where $\varphi_{e\nu}$ is the angle between the electron and neutrino transverse momenta. The M_T fit was used to extract the W mass since it has the greatest statistical power and is the least sensitive to certain systematic effects, notably the production model.

II. EVENT SELECTION

Both $W \rightarrow e\nu$ and $Z \rightarrow ee$ decays are used in the analysis. The electrons from these decays tend to be isolated and of high transverse momentum. At the trigger level (5), W candidates were required to have an electromagnetic object with transverse energy $E_T \geq 20 \text{ GeV}$ and to have missing transverse energy $\cancel{E}_T \geq 20 \text{ GeV}$ for Run 1a and $\cancel{E}_T \geq 15 \text{ GeV}$ for Run 1b. Here $\cancel{E}_T = |\sum_i \vec{E}_i \sin \theta_i|$, with the sum extending over all calorimeter cells. Z candidates were required to have two electromagnetic clusters, each with $E_T \geq 10 \text{ GeV}$.

Each electron candidate was subjected to offline selection criteria to improve the sample purity. The transverse and longitudinal shower profile of the cluster were required to be consistent with that expected for an electron, based upon Monte Carlo simulations and test beam measurements (6). The energy leakage of the cluster into the hadronic compartment of the calorimeter was required to be less than 10% of the cluster energy. Also, the cluster was required to be isolated. The total energy within a cone of radius $R = 0.4$ (7), centered on the electron direction but outside the core of the shower with $R = 0.2$, was required to be less than 15% of the EM energy in the core. A spatial match of the cluster with a central detector track was required. These electron identification criteria were chosen to remove from the sample most of the background events from QCD processes.

Fiducial criteria were also imposed to ensure that the electron candidates were well measured. Electron candidates with cluster position close to the end walls of the cryostat or close to the boundaries between the central calorimeter modules were eliminated from the data sample. These fiducial cuts were chosen based on test beam and Monte Carlo studies of the position dependence of the electron response and reconstruction efficiency.

Having found events with well-identified, isolated electrons and, for W bosons, significant missing transverse energy, further kinematic constraints were imposed. The transverse energies of both electrons in Z events and the electron and neutrino in W events were required to exceed 25 GeV. The neutrino transverse energy was inferred from the total transverse energy balance and was equated to the missing transverse energy. In addition, the transverse momentum of the W boson, p_T^W , had to be less than 30 GeV/c.

III. FAST MONTE CARLO MODEL

The observed M_T distribution is used to extract M_W by a maximum likelihood fit. A fast Monte Carlo (MC) model is used to predict M_T spectra as a function of the W mass. These spectra provide the likelihood functions necessary for the fit. The fast MC model begins with a theoretical calculation of W or Z production and decay at the 4-vector level. Relevant detector effects are simulated. These include the electron angle and energy response and resolutions, scale and resolution of the hadronic recoil system which balances the P_T of the W or Z , kinematic and fiducial acceptances, trigger and selection efficiencies and underlying event effects.

Only the most important features of the model are discussed. These include the modelling of the electron angle and energy and the transverse recoil vector. These correspond to the experimentally independent measurements. From these the neutrino transverse momentum is inferred.

A. Theoretical model

The starting point for the fast simulation is production of W or Z bosons according to a theoretical calculation (10) of $d^2\sigma/dp_T dy$ which includes a resummation of the leading divergences in $1/p_T^2$ as $p_T \rightarrow 0$. The calculation depends on parton distribution functions (pdf) and on a cutoff function S_{NP} which parametrizes non-perturbative physics at very small momenta. We use MRSA pdf (11). S_{NP} has been parametrized and constrained (10) using published Drell-Yan data from several experiments. The spectrum $d^2\sigma/dp_T dy$ determines the distributions of transverse and longitudinal momenta of the vector boson.

The mass of the W or Z is generated according to a relativistic Breit-Wigner lineshape with a skewing from the decrease of parton luminosity with increasing mass. The W width is fixed to its measured value, $\Gamma_W = (2.06 \pm 0.06) \text{ GeV}/c^2$ (5). The decay products are generated with angular distributions respecting the boson polarization.

There are small correlation effects between the mass, P_T , rapidity and polarization of the W or Z boson due to parton luminosity effects. The effect of these correlations on the transverse mass fit has been checked with the RESBOS generator (17) and found to be small.

Radiative decays are generated according to the calculation of Berends and Kleiss (12). For a fraction of the events $W \rightarrow \tau\nu \rightarrow e\nu\nu\nu$ decays are generated. With each simulated event there is also associated an event vertex position and an instantaneous luminosity which are used subsequently in the detector simulation.

The product of the theory stage of the simulation is a set of "true" 4-vectors which describe the event kinematics. The most important of these quantities are the true electron momentum and true recoil vectors, which when smeared and subjected to selection criteria, correspond to the quantities reconstructed in the detector and used to calculate the W transverse mass or Z invariant mass.

B. Electron measurement and modelling

The electron polar angle is computed from two points on the trajectory, the center of gravity of the calorimeter cluster and the center of gravity of the matched track in the central drift chamber. The calorimeter position finding algorithm was studied with test beam data and detailed Monte Carlo simulations. The central drift chamber has been calibrated using muons from both collider data and cosmic rays. The resolution of the polar angle defined in

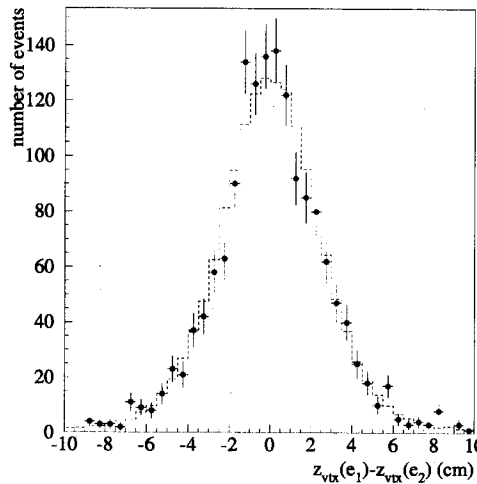


FIG. 1. Comparison of the $z_1 - z_2$ distribution for the $Z \rightarrow ee$ data (points) and the fast MC model (dashes).

this way is determined from $Z \rightarrow ee$ data. The two electron trajectories are extrapolated to the beam axis to give two independent estimates of the event vertex, z_1 and z_2 . The polar angle resolution is then extracted from the distribution of the difference $z_1 - z_2$, shown in figure 1.

In modelling the electron energy response, we use the relationship between the energy measured in the calorimeter and the true energy $E_{\text{meas}} = \alpha E_{\text{true}} + \delta$. This relationship is derived from test beam studies. The energy offset term, δ , allows for a nonlinearity in the electron response, defined as $E_{\text{meas}}/E_{\text{true}}$. Two complementary approaches are used to constrain the energy response.

The first approach is based entirely on $Z \rightarrow ee$ decays and exploits the variation in energy of the electrons from $Z \rightarrow ee$ decays. The measured and true mass values are, to first order, related to each other by $m_{\text{meas}} = \alpha m_{\text{true}} + \delta f$. The variable f depends on the decay topology and is given by $f = \frac{2(E_1 + E_2)}{m_{\text{true}}} \sin^2 \gamma/2$, with γ the opening angle between the two decay products and E_1 and E_2 their energies. A fit to the Z mass as a function of f provides a measurement of both the scale, α , and offset, δ .

In the second approach, the Z resonance is used in conjunction with $\pi^0 \rightarrow \gamma\gamma$ and $J/\psi \rightarrow e^+ e^-$ decays, and the precisely known masses of these three resonances (8). Figure 2 shows the π^0 and J/ψ signals observed at DØ. Both photons from a π^0 decay are required to convert so that we can measure the opening angle using the conversion tracks. However, the two photons are not resolved into separate clusters, so an invariant mass is not reconstructed. Instead we define the “symmetric mass,” M_{sym} , to be the invariant mass computed as if the two photons had shared the cluster energy equally. The energy scale and offset are extracted by comparing the observed M_{sym} spectrum to a Monte Carlo simulation of the M_{sym} lineshape. Figure 3 shows the Z invariant mass spectrum.

By combining the information from these methods we obtain an excellent constraint on the EM response. Figure 3 shows the constraints on the parameters α and δ from the π^0 data, the J/ψ data, and the complementary approach using just the Z events. When combined, these three independent constraints limit α and δ to the small elliptical region. Test beam measurements allows for a small nonlinear term in the energy response in addition to that

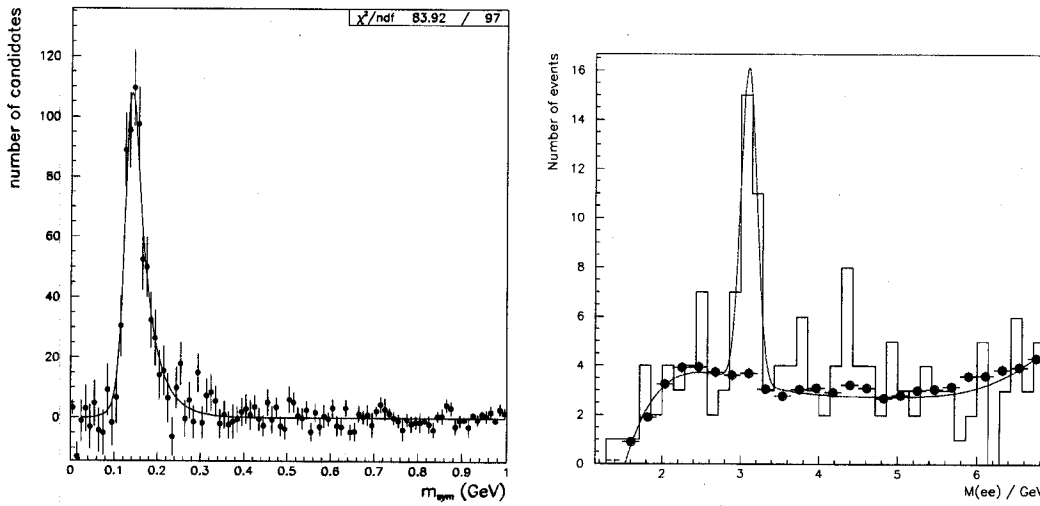


FIG. 2. (Left) π^0 symmetric mass distribution. (Right) J/ψ invariant mass distribution.

due to the offset. Allowing such an additional term affects the determination of both the offset and the scale and alters the ratio of (M_W/M_Z) largely through the effect on δ . This has been included in the determination of the scale error. The dependence of the measured ratio of the W mass to Z mass on α and δ may be estimated from the equation

$$\left. \frac{M_W(\alpha, \delta)}{M_Z(\alpha, \delta)} \right|_{\text{meas}} = \left. \frac{M_W}{M_Z} \right|_{\text{true}} \left[1 + \frac{\delta}{\alpha} \cdot \frac{f_W M_Z - f_Z M_W}{M_Z \cdot M_W} \right].$$

It should be noted that the W mass is insensitive to the energy scale α if δ is small. The offset results in a small correction to the measured mass. The uncertainty on the absolute energy scale results in an uncertainty on M_W of 160 MeV/c² for the Run 1a data and 80 MeV/c² for the Run 1b data. In both cases the uncertainty is dominated by the limited statistical accuracy of the measured Z mass.

To improve the EM energy resolution, the relative calibration of the energy response of the 32 central electromagnetic (EM) calorimeter modules was performed using a sample of inclusive EM clusters to a relative precision of $\approx 0.5\%$. The electromagnetic energy resolution was derived from the width of the observed $Z \rightarrow ee$ resonance, using the previously measured angular resolutions and the precisely known value of Γ_Z (9) from LEP.

C. Recoil vector measurement and modelling

The relative response of the hadronic calorimeter with respect to the EM calorimeter is established by studying Z events. We denote this relative response α_{rec} . Figure 4 shows the imbalance between the P_T of the Z boson measured with the electrons, \vec{P}_T^{ee} , relative to the P_T measured with the hadronic system, \vec{u}_T . Both are projected onto the η axis, defined as the axis in the transverse plane bisecting the transverse momentum vectors of the two electrons. This η -projection is used to minimize the effects of the electron resolutions. If the electron and hadron energy scales were the same this plot would be flat. A linear dependence is observed, indicating a relative scale between the electron and hadron measurements. From

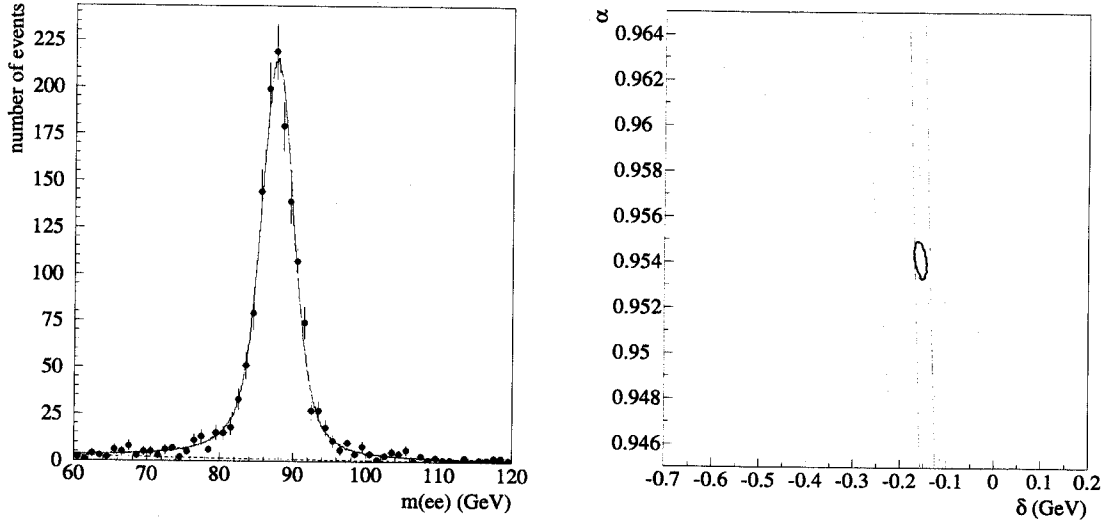


FIG. 3. (Left) $Z \rightarrow ee$ invariant mass distribution. (Right) Constraints on slope α and intercept δ from observed $J/\psi \rightarrow e^+e^-$ (dotted line), $\pi^0 \rightarrow \gamma\gamma$ (dashed line), and $Z \rightarrow e^+e^-$ decays (dashed-dotted line). The shaded inner contour shows the combined result.

the Run 1a $Z \rightarrow ee$ data the measured scale factor was (0.83 ± 0.04) , while from the Run 1b data the corresponding factor was (0.81 ± 0.015) . To ensure an equivalent event topology between the W and Z events, Z decays in which one electron is in the end calorimeter were included in this study.

The measured recoil vector can be modelled as a sum of two components. The first is a vector parallel to the true boson P_T which is reconstructed with a scale α_{rec} relative to the EM scale. The second component is a vector symmetrically distributed with respect to the boson P_T direction. Intuitively, the first component corresponds to a recoil jet and the second to a resolution vector which combines the effects of the underlying event debris from spectator partons in the boson production interaction, calorimeter noise, particles from multiple interactions in the same beam crossing as the W or Z event and pileup effects from previous interactions. We model the asymmetric component by scaling the true P_T by a scale α_{rec} and applying a resolution with a constant term of 4% and a sampling term of S_{rec} . We model the symmetric component using collider minimum bias events with a luminosity distribution chosen so that the mean number of interactions is the same as the mean number of interactions in the W sample. We scale the \vec{P}_T vector from the minimum bias events by a factor α_{mb} . We constrain the pair of parameters S_{rec} and α_{mb} by comparing the P_T measured with the electrons and the hadrons after correcting for the relative response of the electron and hadron measurements. The projection of that difference onto the η axis, $(\vec{P}_T^{ee} + \vec{P}_T^{rec}/\alpha_{rec}) \cdot \hat{\eta}$, is called the η balance. The width of this variable is denoted σ_η . The contributions of S_{rec} to σ_η increases with P_T^{ee} while that of α_{mb} is constant with P_T^{ee} , hence both terms can be measured from the $Z \rightarrow ee$ data by studying σ_η as a function of P_T^{ee} . Figure 5 shows the relative contributions of the resolutions of the symmetric and asymmetric components and the electron resolution to σ_η . The contribution

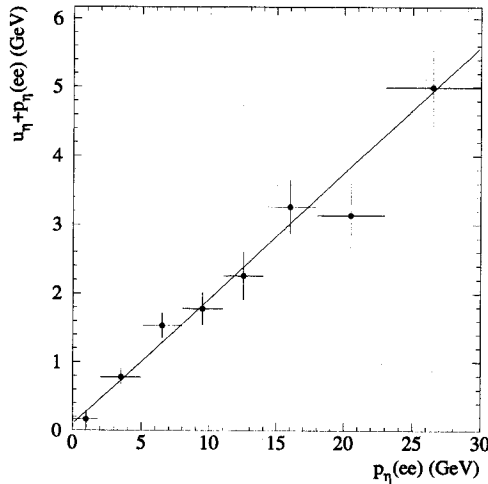


FIG. 4. Comparison of P_T in $Z \rightarrow ee$ events measured with electrons with the hadronic measurement

from the electrons is negligible – this is the motivation for using the η axis to study the hadronic resolutions. Figure 6 shows the result of the fit to σ_η for the hadronic resolution parameters S_{rec} and α_{mb} . This fit is performed using the Run 1b $Z \rightarrow ee$ data. For the Run 1a analysis, a similar resolution model is implemented but S_{rec} is derived from dijet resolution studies and α_{mb} from the Run 1a $Z \rightarrow ee$ data. We find that α_{mb} is consistent with unity as expected, for both Run 1a and Run 1b.

IV. DETECTOR AND RECONSTRUCTION BIASES

Significant detector and reconstruction biases were modelled in the Monte Carlo simulation.

The energy underlying the electron was obtained from W events by measuring the energy deposited in a region of the calorimeter the same size as the electron cluster but rotated in azimuth. On average, the underlying event adds (16.7 ± 1.5) MeV per tower ($\Delta\eta \times \Delta\varphi = 0.1 \times 0.1$) to the energy of central electrons. This leads to an uncertainty of 35 MeV/c² on M_W .

In radiative decays, $W \rightarrow e\nu\gamma$, the $e\nu$ mass does not reconstruct to the W mass unless the photon is clustered with the electron. Also, radiative decays in which the photon is radiated near, but not fully within, the electron cluster can distort the cluster shape causing the electron to fail the shower shape cuts. The same considerations apply to radiative Z decays and these effects do not cancel completely in the ratio of masses.

Similarly, the recoil system may affect the electron identification, especially if it is close to the electron. A measure of the event selection biases, through electron shape and isolation cuts, is obtained by studying the projection of the momentum recoiling against the W along the electron p_T direction (\hat{p}_T^e): $u_{\parallel} \equiv \vec{p}_T^{rec} \cdot \hat{p}_T^e$. An inefficiency in u_{\parallel} would cause a kinematic bias for the W decay products. The efficiency as a function of u_{\parallel} has been determined for the Run 1a analysis using the energy distribution in isolation cones around the electrons in W events, and has been verified using Z decays. In an alternative approach used for

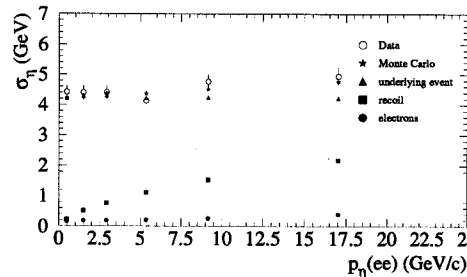


FIG. 5. Contributions of symmetric and asymmetric hadronic resolution components to σ_η , as a function of the η projection $\vec{P}_T^{ee} \cdot \hat{\eta} = P_\eta(ee)$. The three contributions which can be varied in the MC model are from the electrons (solid circles), recoil vector asymmetric resolution (squares), and underlying event symmetric resolution (triangles). The stars show the combined resolution and open circles represent the values measured from the $Z \rightarrow ee$ data.

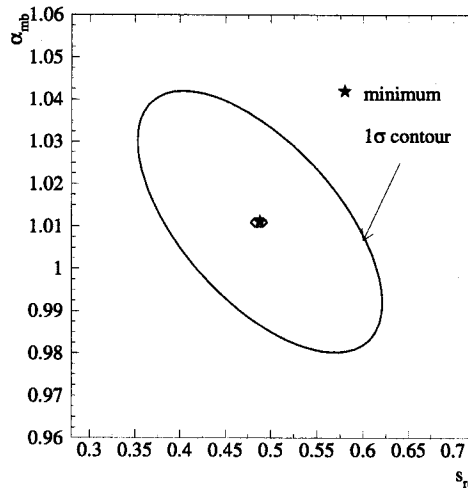


FIG. 6. Allowed region for S_{rec} and α_{mb} .

the Run 1b analysis, Monte Carlo electrons simulated with GEANT were superimposed on events in the W sample, taking into account the appropriate kinematic correlations. The efficiency as a function of $u_{||}$ was determined directly from this hybrid sample. The W mass from the transverse mass fit is largely insensitive to this inefficiency.

V. BACKGROUNDS

The QCD jet background in the W sample was determined from an independent jet data sample to be $(1.6 \pm 0.8)\%$ for the Run 1a sample. Inclusion of this background shifts the mass by $+33$ MeV/c 2 . The corresponding value for the Run 1b sample is $(1.5 \pm 0.3)\%$. The background from $Z \rightarrow e^+e^-$ events in which one electron is not identified has been estimated, using ISAJET (13), to be $\approx 0.5\%$. Its effect on M_W is negligible. The irreducible background due to $W \rightarrow \tau\nu \rightarrow e\nu\nu\nu$ was included in the Monte Carlo simulation. All other

sources of background are negligible.

The contributions of the backgrounds to the transverse mass distribution were accounted for in the fits.

VI. W MASS FITS

The distribution in transverse mass and the Monte Carlo lineshape corresponding to the best fit to the Run 1b data are shown in Fig. 7. The mass from the Run 1a sample, extracted from a fit of the events in the range $60 \leq M_T \leq 90$ GeV/c^2 , is $M_W = 80.35 \pm 0.14$ (stat.) ± 0.17 (syst.) ± 0.16 (scale) GeV/c^2 . The mass from the Run 1b sample, using the same fitting range is $M_W = 80.38 \pm 0.07$ (stat.) ± 0.13 (syst.) ± 0.08 (scale) GeV/c^2 .

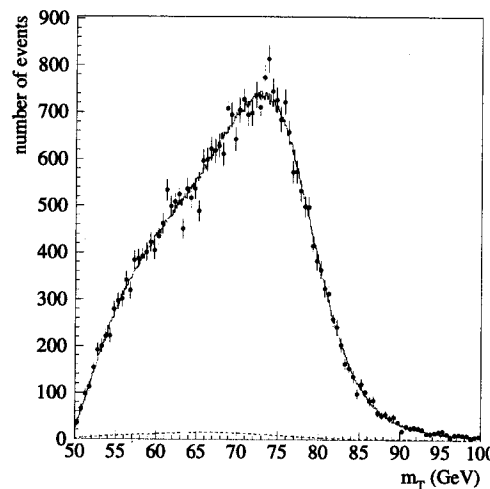


FIG. 7. The transverse mass distribution for the Run 1b W sample. The points indicate the data, the solid line the simulated M_T lineshape for the best fit, and the dashed line the background contribution.

Table 2 lists the uncertainties in the measurements. The χ^2 statistic for the Run 1a M_T fit is 18.6 for 29 degrees of freedom. For the Run 1b fit the χ^2 is 87 for 59 degrees of freedom. The large value of χ^2 is due to four M_T bins with $|\chi| > 2.5$. These four points are scattered over the fitting window and there do not appear to be any systematic correlations between them. We have performed a Kolmogorov-Smirnov test to determine the probability that the fit and the data come from the same parent distribution and obtain a probability of 95%. The fitted mass is insensitive to the choice of fitting window for a large range of values of both the upper and lower M_T limits. We conclude that the data M_T spectrum is well reproduced by the model.

Due to the preliminary nature of the Run 1b fit we have chosen not to combine the Run 1a and Run 1b results. Some of the errors are correlated between the two measurements.

VII. SYSTEMATIC ERRORS

In general, systematic errors were estimated by varying the assumptions of the Monte Carlo model and determining the sensitivity of the W mass fit to each of the inputs to the

model. For example, from the width of the Run 1b $Z \rightarrow ee$ invariant mass distribution, the constant term in the electron energy resolution was measured to be $(0.9^{+0.30}_{-0.45})\%$. The systematic error due to the electron energy resolution is determined by evaluating the variation of the fitted mass over the allowed range of the energy resolution from this measurement. A similar procedure has been carried out for the various parameters used in the MC model listed in Table 2.

For the Run 1b result, the data are collected over a wide range of instantaneous luminosities. The mass shift observed when events collected at luminosities greater than $9 \times 10^{30} \text{ cm}^{-2} \text{ s}^{-1}$ are eliminated from the sample is $70 \text{ MeV}/c^2$. We conservatively include a systematic error of $70 \text{ MeV}/c^2$ to account for possible inadequacies of the modelling of very high luminosity events. Extensive cross checks of the luminosity dependence incorporated into the fast Monte Carlo model are in progress, and it is anticipated that this uncertainty will not contribute to the systematic error in the final result.

One of the large systematic uncertainties is due to the model of the p_T^W spectrum and the pdf's. The correlation between the pdf's and the p_T^W distribution has been addressed. The pdf's are constrained by the measured HERA data (14) and W charge asymmetry (A_W) (15). New parametrizations of the CTEQ3M pdf were obtained incorporating all available data with the A_W data points moved coherently by \pm one standard deviation. The parameters governing the non-perturbative part of the p_T^W spectrum (16) were varied simultaneously, as constrained by our measured Run 1a p_T^Z spectrum. The resulting variation in the W mass leads to an uncertainty of $65 \text{ MeV}/c^2$ on M_W . Work is in progress to further constrain the production model using Run 1b data. It is expected that this contribution to the systematic uncertainty will be reduced in the final result.

Uncertainty	Run 1a	Run 1b
	MeV/ c^2	
Statistical	140	70
Energy scale	160	80
p_T^W , pdf	65	65
# of Min Bias events	60	40
Angle Calibration	50	40
Hadronic Energy Scale	50	30
EM Energy resolution	70	30
Underlying Event	35	30
Hadronic Energy Resolution	65	20
Efficiencies	30	20
Radiative Decays	20	20
Backgrounds	35	15
W Natural Width	20	10
Calorimeter non-uniformity	10	10
Fit Error	5	5
Luminosity dependence		70
Total Systematic	165	130
Total	270	170

TABLE 2. Uncertainties in the W boson mass measurement

VIII. CONCLUSION

Preliminary measurements of the W boson mass from the transverse mass spectrum of central $W \rightarrow e\nu$ decays from Run 1a and Run 1b are presented. The preliminary results are $M_W = 80.35 \pm 0.27 \text{ GeV}/c^2$ from Run 1a and $M_W = 80.35 \pm 0.17 \text{ GeV}/c^2$ from Run 1b.

ACKNOWLEDGMENTS

We thank the staffs at Fermilab and the collaborating institutions for their contributions to the success of this work, and acknowledge support from the Department of Energy and National Science Foundation (U.S.A.), Commissariat à L'Energie Atomique (France), Ministries for Atomic Energy and Science and Technology Policy (Russia), CNPq (Brazil), Departments of Atomic Energy and Science and Education (India), Colciencias (Colombia), CONACyT (Mexico), Ministry of Education and KOSEF (Korea), CONICET and UBACyT (Argentina), and the A.P. Sloan Foundation.

REFERENCES

- * Visitor from IHEP, Beijing, China.
- † Visitor from Univ. San Francisco de Quito, Ecuador.
- 1. S. Weinberg, Phys. Rev. Lett. **19**, 1264 (1967); S.L. Glashow, Nucl. Phys. **22**, 579 (1968); A. Salam, in *Elementary Particle Theory*, ed. by N. Svartholm (Almqvist and Wiksell, Sweden, 1968), p. 367; S.L. Glashow, J. Iliopoulos and L. Maiani, Phys. Rev. D **2**, 1285 (1970); M. Kobayashi and M. Maskawa, Prog. Theor. Phys. **49**, 652 (1973).
- 2. Other recent measurements are J. Alitti *et al.* (UA2 Collaboration), Phys. Lett. **B276**, 354 (1992); F. Abe *et al.* (CDF Collaboration), Phys. Rev. Lett. **65**, 2243 (1990), Phys. Rev. D **43**, 2070 (1991); F. Abe *et al.* (CDF Collaboration), Phys. Rev. Lett. **75**, 11 (1995), F. Abe *et al.* Phys. Rev. **D52**, 4784 (1995).
- 3. S. Abachi *et al.* (DØ Collaboration), *Nucl. Instr. and Methods* **A338**, 185 (1994).
- 4. Pseudorapidity is defined as $\eta = -\ln \tan \frac{\theta}{2}$ where θ is the polar angle with respect to the proton beam.
- 5. S. Abachi *et al.* (DØ Collaboration), Phys. Rev. Lett. **75**, 1456 (1995).
- 6. For more details, see S. Abachi *et al.* (DØ Collaboration), Phys. Rev. D **52**, 4877 (1995).
- 7. R is defined as $R = \sqrt{\Delta\eta^2 + \Delta\varphi^2}$ where $\Delta\eta$ and $\Delta\varphi$ are calculated from the center of the calorimeter cells with respect to the (η, φ) position of the electromagnetic shower.
- 8. The reference mass values used are $M_Z^{\text{LEP}} = 91.1884 \pm 0.0022 \text{ GeV}/c^2$, from P. Renton, "Precision Tests of Electroweak Theories," Lepton-Photon Conference, Beijing, P.R. China (1995), OUNP-95-20; $M_{J/\psi} = 3.09688 \pm 0.00004 \text{ GeV}/c^2$ and $M_{\pi^0} = 0.135 \pm 0.0006 \text{ GeV}/c^2$, Particle Data Group, L. Montanet *et al.*, Phys. Rev. D **50**, 1173 (1994).
- 9. Particle Data Group, L. Montanet *et al.*, Phys. Rev. D **50**, 1173 (1994).
- 10. G. Ladinsky and C.P. Yuan, Phys. Rev. D **50**, 4239 (1994).
- 11. A.D. Martin, R.G. Roberts and W.J. Stirling, Phys. Rev. D **50**, 6734 (1994); A.D. Martin, R.G. Roberts and W.J. Stirling, Phys. Rev. D **51**, 4756 (1995).
- 12. F. A. Berends and R. Kleiss, Z. Phys. **C27**, 365 (1985).
- 13. F. Paige and S. Protopopescu, BNL Report no. BNL38034 (1986, unpublished), release v 6.49.
- 14. M. Derrick *et al.* (ZEUS Collaboration), Phys. Lett. **B316**, 412 (1993); I. Abt *et al.* (H1 Collaboration), Nucl. Phys. **B407**, 515 (1993).
- 15. F. Abe *et al.* (CDF Collaboration), Phys. Rev. Lett. **74**, 850 (1995).

